RESEARCH ARTICLE

Macromolecular Materials and Engineering
www.mame-journal.de

Nozzle-Pressurized Gyration: A Novel Fiber Manufacturing Process

*Yanqi Dai, Jubair Ahmed, Angelo Delbusso, and Mohan Edirisinghe**

An innovative development of pressurized gyration is presented, incorporating a directional nozzle system. Thus, nozzle-pressurized gyration is used to prepare polymeric fibers. In this work, three different polymeric fibers (polycaprolactone, polyvinylpyrrolidone, and polyethylene oxide) manufactured by the original pressurized gyration and nozzle-pressurized gyration are compared. Under the same processing parameters (working pressure, rotational speed, and collection distance), nozzle-pressurized gyration is proved to be a highly efficient spinning technology for uniform and uniaxially oriented fiber products. The effects of the spinning vessel geometry on the morphology and alignment of gyrospun fibers are elucidated. This work also reveals the relationship between fiber morphology and collection distance in nozzle-pressurized gyration. Varying the collection distance provides a useful approach to the synthesis of uniform fibers with anisotropic arrangement.

1. Introduction

Polymeric fibers have been widely used in biomedical applications, for example, sustained release systems for drug delivery, functional scaffolds especially in tissue engineering and antibacterial bandages for wound healing, due to their unique structural characteristics and inherent properties.[1–4] Especially during the SARS-CoV-2 pandemic, fibers with very small diameter have become one of promising candidates for medical protective equipment, face masks, protective suits, etc. Fine fibers act as the effective filter media for microorganisms (bacteria, viruses and fungi) due to their large surface area to volume ratio, microscopic pores and specific porosity. The unique surface effects of nanofibers show excellent anti-microbial properties through collision or capture with tiny particles (micro- or nanoscale).[5]

Y. Dai, J. Ahmed, A. Delbusso, M. Edirisinghe
Department of Mechanical Engineering
University College London
Torrington Place, London WC1E 7JE, UK
E-mail: m.edirisinghe@ucl.ac.uk

The ORCID identification number(s) for the author(s) of this article can be found under https://doi.org/10.1002/mame.202200268

DOI: 10.1002/mame.202200268

Although the research on fiber manufacturing technologies has been progressing for hundreds of years, it is still a topic which draws very significant attention in industrial and academic circles.[6] These efforts have been mainly focused on the reduction of fiber size and the increase of fiber yield. Ultrafine fibers with the diameter smaller than 100 nm have been fabricated by facile methods.[7–9] As the quality and quantity of polymeric fibers have increased to a satisfactory degree, much attention has been paid to the customization of fiber structures and functions. Through technological innovation and parameter optimization, polymeric fibers with uniform, beaded, hollow, core-sheath, and porous structures have been successfully prepared in laboratories.[10–14]

Theoretically, an ideal uniform fiber means that there is no variation in the fiber diameter along the fiber length of individual fiber strands.[15] Compared with beaded fibers, uniform fibers show superior mechanical properties. Many reports have demonstrated that the presence of beads and defects on fibers considerably reduces the cohesion between fibers, resulting in lower Young's modulus, tensile strength, and elongation at break.[16–18] In addition, seeding cells on highly aligned fiber scaffolds tends to be more effective than that on randomly oriented fiber scaffolds, in order to achieve cell orientation control in tissue engineering.[17,19,20] This is related to the regular and defined orientation architecture of the natural extracellular matrix (ECM) found in tissues and organs.[21] The studies from Ottosson et al. and Norzain and Lin have shown that the anisotropic orientation of fibers has significant impacts on cell adhesion mechanisms and promotes elongation and migration of fibroblasts along the fiber direction.[22–24] The results suggest that the aligned fiber scaffold is a highly promising candidate for biomedical applications.

Electrospinning is one of the most widely used fiber fabrication technologies. It overcomes the surface tension of polymer solutions in a high-voltage electric field, forming randomly arranged fibers.[25] To obtain uniform and uniaxially oriented fibers, researches were focused on the optimization of spinning parameters, needle design and complex components of the collector used in electrospinning.[26–34] However, the inherent limitations of electrospinning remain, such as high energy consumption, low productivity, and limited options of electrospinning conductive solutions.[35–37]

To solve the challenges faced by electrospinning, nonelectric field-driven spinning technologies have gradually attracted

attention and are recognized as highly efficient fiber making strategies.[37–40] Pressurized gyration (PG), proposed in 2013, is a spinning technology that combines centrifugal force and solution blowing for mass production of fibers.[41] The original PG setup has a perforated cylindrical vessel connected to an electrical motor and a gas inlet.[42] When the vessel rotates at a certain speed, the loaded liquid forms a vortex at the bottom of the vessel. The liquid moves to the side walls of the vessel. The liquid–gas interface is parabolic.[43] When the centrifugal force is able to overcome the surface tension of the liquid, the liquid is ejected from the vessel orifices. Moreover, a surface tension gradient occurs at the liquid–gas interface, resulting in a Marangoni stress tangential to the liquid–gas interface.[44] The stress carries the fluid toward the tip of the droplet.[41] The droplets leaving the vessel are continuously stretched and elongated under the action of inertia, surface tension and pressure differential, forming liquid jets.[45] During this process, the solvent evaporates and dry polymer fibers are produced.[46,47] In PG, the high-pressure nitrogen stream affects the surface profile of the fluid, the time required for the process, and the fiber diameter.[43] This is due to the kinetic energy of the gas flow, which increases the velocity of the polymer fluid and creates a large pressure differential in the vessel, leading to the greater initial velocity and acceleration of the polymer fluid, as it flows through the orifices. In addition, the gas pressure facilitates the jet elongation, producing fibers with a smaller diameter. PG is an encouraging innovation in polymer forming, which has been reported to successfully manufacture homogeneous fibers, core-sheath fibers, drug-loaded fibers, encapsulated nanoparticles and other nanopolymer materials with specific morphology.[1,41,45,48–52]

In this work, we report a novel nozzle-PG setup for the first time. It effectively improves the uniformity and orientation of produced fiber products. In nozzle-PG, the nozzles direct the polymer solution flow when it's ejected. We compare the differences in the morphology and alignment of fibers produced by PG and nozzle-PG to demonstrate the potential of nozzle-PG in producing uniform and highly aligned fibers. To study the optimal spinning parameters for the manufacture of desired fibers, this work also reveals the effects of working pressure and collection distance on the fiber morphology obtained in nozzle-PG.

2. Experimental Section

2.1. Materials

Polycaprolactone (PCL, Mw ≈ 80 000 g mol^{-1}, CAS: 24980-41-4), polyvinylpyrrolidone (PVP, Mw ≈ 1 300 000, CAS: 9003-39-8), and polyethylene oxide (PEO, Mw ≈ 200 000, CAS: 25322-68-3) were obtained from Sigma-Aldrich (Gillingham, UK). The solvents used: ethanol absolute (CAS: 64-17-5) was purchased from VWR Chemicals (Strasbourg, France) and chloroform (CAS: 67-66-3) was purchased from Sigma-Aldrich (Gillingham, UK). All chemicals were of analytical grade and were used as received.

2.2. Preparation and Characterization of Polymer Solutions

PCL pellets were dissolved in chloroform and stirred magnetically at ambient temperature (≈20 °C) for 24 h to obtain a homogeneous 15% (w/v) PCL solution. 15% (w/v) PVP solution and 15% (w/v) PEO solution were prepared by dissolving PVP powders and PEO powders in ethanol and distilled water, respectively, and processing under the same conditions. The surface tension and viscosity of the three polymer solutions were characterized using a calibrated Kruss Tensiometer and a Brookfield Viscosity-meter, respectively. The characteristics of polymer solutions used in this study are summarized in **Table 1**.

Table 1. Polymer type, concentration, solvent, surface tension, and viscosity of the three solutions at ambient temperature.

Polymer	% (w/v)	Solvent	Surface Tension [mN m^{-1}]	Viscosity [mPa s]
PCL	15	Chloroform	32.7 ± 0.3	2065.0 ± 35.8
PVP	15	Ethanol	24.6 ± 0.2	751.8 ± 6.1
PEO	15	Distilled water	58.1 ± 0.4	2144.3 ± 74.9

2.3. Design of Spinning Vessels

The experimental setups for fiber forming used in this study are original PG and nozzle-PG. **Figure 1**a shows that the gas inlet and an electrical motor were connected to an aluminum gyrospinning vessel with equal-distanced 24 orifices in the original PG setup. The diameter of the orifices is 0.5 mm. For the nozzle-PG setup, the vessel is equipped with four equally spaced nozzles with the inner diameter of 0.5 mm and the length of 5 mm (Figure 1b). The orifices and the nozzles are placed 15 mm upward from the vessel base. The gyrospinning vessels of PG and nozzle-PG have the identical height and internal diameter (cylindrical vessel, 35 mm × 60 mm).

2.4. Manufacturing Polymer Fibers

According to previous reports,[41,51] for an individual spinning experiment, 3 mL of the same polymer solution was loaded into the chambers in PG and nozzle-PG for spinning under the specific working pressure and collection distance. Each round of spinning was performed at 13 000 rpm under the same ambient temperature (≈20 °C) and relative humidity (≈50%). The spinning parameters of all fiber samples are listed in **Tables 2** and **3**.

2.5. Fiber Characterization

The fibers were imaged using a Hitachi S3400N Scanning Electron Microscope (SEM, Japan). All samples were coated with gold using a Quorum Q150R ES sputtering machine (UK) for 150 s to minimize charging effects before imaging. ImageJ (software) was used to measure the fiber diameter. For each fiber sample, a total of 300 measurements were obtained. To better indicate fiber uniformity, diameter was measured at 10 points along the length of each single fiber randomly picked. This was repeated on 30 different fibers for each fiber sample. The mean and the standard deviation of fiber diameter were calculated. The mean value reflects the size of fibers. The value of standard deviation can be used as an indicator of fiber uniformity, reflecting not only the

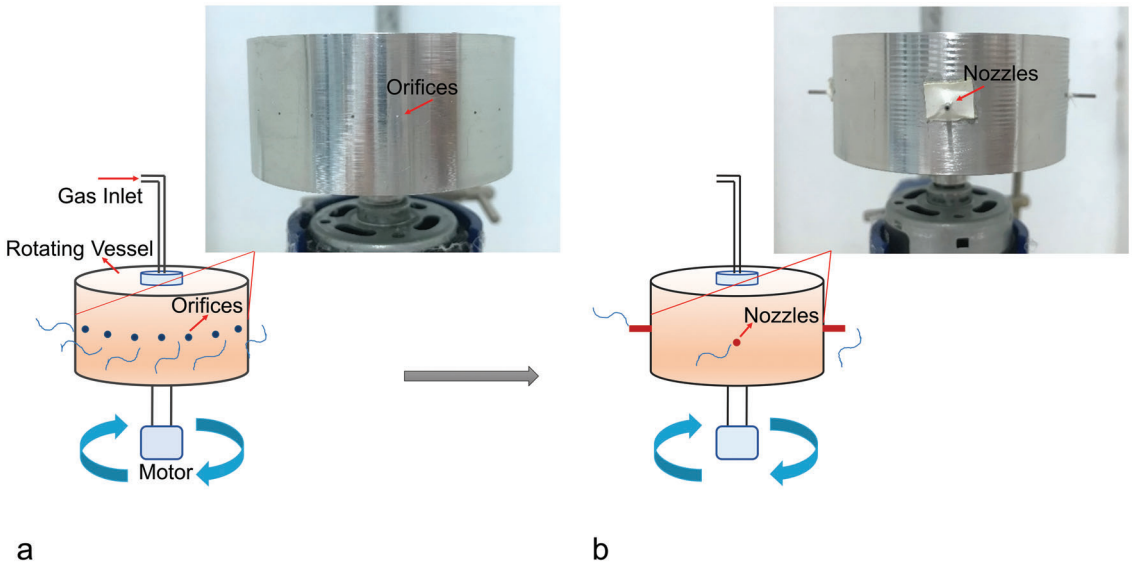

Figure 1. Schematic diagrams and actual pictures of a) original PG setup with 24 orifices and b) nozzle-PG setup with 4 external nozzles.

Table 2. Spinning parameters of fiber samples processed by PG and nozzle-PG with the collection distance of 100 mm.

Polymer	Fiber production method	Working pressure [MPa]
PCL	PG	0.1, 0.2, 0.3
	Nozzle-PG	0.1, 0.2, 0.3
PVP	PG	0.1, 0.2, 0.3
	Nozzle-PG	0.1, 0.2, 0.3
PEO	PG	0.1, 0.2, 0.3
	Nozzle-PG	0.1, 0.2, 0.3

Table 3. Spinning parameters of fiber samples collected at different distances in nozzle-PG.

Polymer	Working pressure [MPa]	Collection distance [mm]
PCL	0.1	70, 100, 130
PVP	0.1	70, 100, 130
PEO	0.1	70, 100, 130

uniformity of an individual fiber, but also the variation of diameter between different fibers. The fiber diameter frequency distributions were obtained by OriginPro (software). OrientationJ (ImageJ plugin) was used to construct the distribution of fiber orientation and calculate the directional coherence coefficient of fibers. The coherence coefficient is an index between 0 and 1. A directional coherence coefficient close to 1 indicates a high fiber orientation.[53]

3. Results and Discussion

3.1. Fiber Diameter and Morphology

It can be clearly seen that under the same solution system and spinning parameters, nozzle-PG produced a PCL fiber mat without beads, while the PCL fibers obtained from original PG were randomly arranged with large beads (**Figure 2**a,d). From the inset in Figure 2d, we can see that the nozzle-PG produced PCL fibers with smooth and more uniform morphology. On the contrary, PG-processed PCL fibers were nonuniform (Figure 2a). The fiber diameter distribution graphs (Figure 2b,e) illustrate that PCL fibers obtained from nozzle-PG had smaller fiber diameter and narrower diameter distribution than those obtained from PG, with the mean of 2.4 μm and the standard deviation of 1.2 μm. PG-produced PCL fibers have a diameter of 3.9 ± 2.4 μm. In addition, PCL fibers obtained by nozzle-PG had a larger orientation coherence (0.58) than that of PG fibers (0.36), indicating the better alignment of PCL fibers obtained from nozzle-PG.

Similar results were obtained from the spinning under 0.2 and 0.3 MPa pressures. PCL fiber mats fabricated by PG were randomly arranged with the presence of some thicker fibers and large beads (**Figures 3**a and **4**a). While nozzle-PG produced PCL fibers with more aligned orientation and less beads (Figures 3d and 4d). The PCL fibers had the diameter of 2.8 ± 2.8 μm at 0.2 MPa for PG and 2.1 ± 1.1 μm at 0.2 MPa for nozzle-PG, suggesting that nozzle-PG enabled the manufacture of thinner and more uniform fibers. The orientation coherency coefficient of fibers produced by 0.2 MPa nozzle-PG (0.46) is closer to 1 than that of PG (0.20), indicating its higher alignment.[54] Similar results can also be acquired from the spinning under 0.3 MPa working pressure (Figure 4). These results show that even under different working pressures, nozzle-PG always produced thinner and more uniform PCL fibers with aligned arrangement than those obtained from original PG. These effects can be explained by the stability of spinning jets. Although the polymer solution undergoes a similar trajectory after moving out of the vessel in nozzle gyrospinning and nozzle-free gyrospinning, including jet necking, whipping, and formation of an anti-S shape jet path, the direction of the jet ejection and the flow state of the polymer solution are different.[55,56] In PG, the gas outflow path from the orifices is jet-like (**Figure 5**a).[57] In addition, turbulence occurs due to the chaotic change in pressure when the polymer fluid

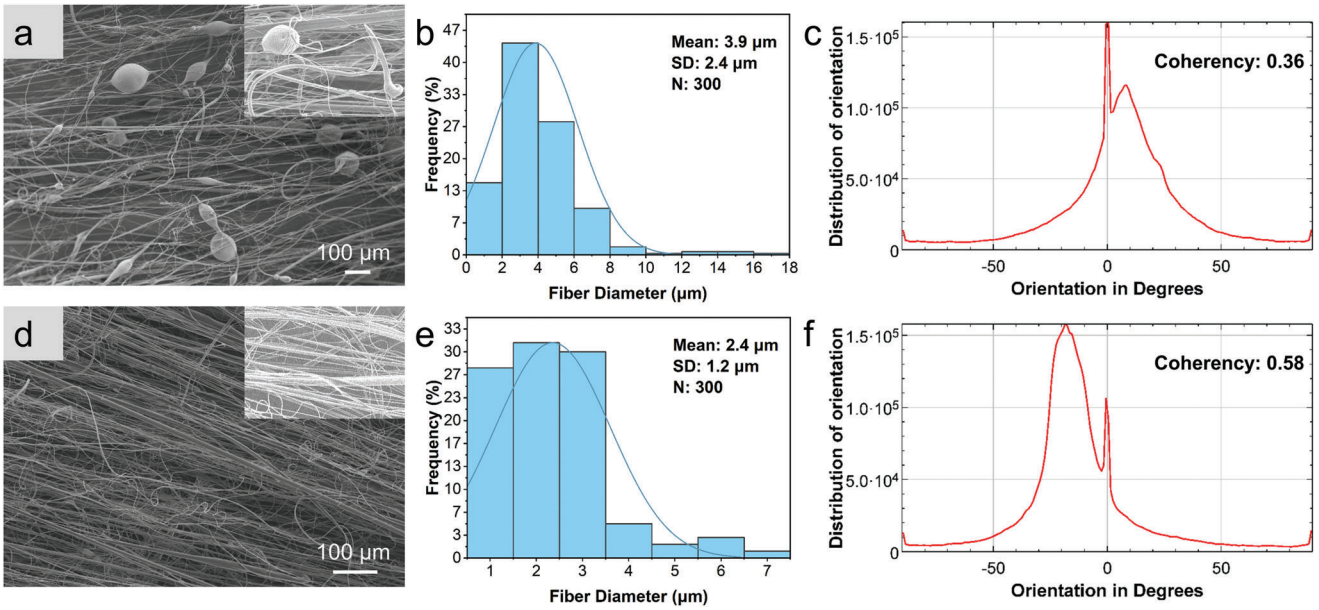

Figure 2. SEM images, fiber diameter distribution graphs, and orientation distribution graphs of PCL fibers produced by a–c) PG and d–f) nozzle-PG under 0.1 MPa working pressure. The insets show the high-magnification (×500) SEM images of fibers.

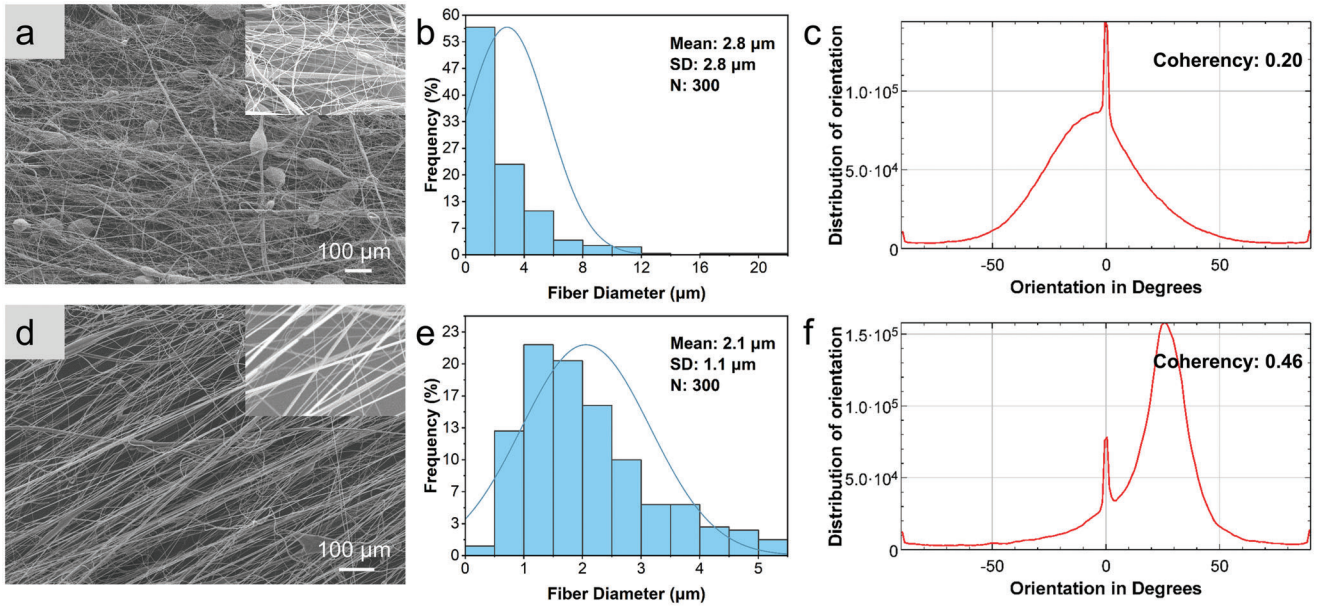

Figure 3. SEM images, fiber diameter distribution graphs, and orientation distribution graphs of PCL fibers produced by a–c) PG and d–f) nozzle-PG under 0.2 MPa working pressure. The insets show the high-magnification (×600) SEM images of fibers.

is ejected through the orifices.[58] This means that the polymer jets may be formed with a certain angle to the central axis of the orifice and have different initial jet diameters (Figure 5b).[59] It explains the lower alignment and uniformity of PG fiber products. However, when the fluid flows through the nozzles, it is subjected to the centrifugal force (F_{cent}), the static pressure (F_p), the viscous force (F_τ), and the surface tension (F_s) parallel to the axis of the nozzle, which help it move along the length of the nozzle (Figure 5c).[56] Moreover, directing the liquid by nozzles helps to stabilize the flow state of the polymer flow and form stable spinning jets.[60] Finally, the polymer jets leave the nozzle in a more stable flow state and tend to move along the nozzle axis under the action of inertia, thereby improving the alignment and uniformity of fibers.

Through the comparison of Figures 2–4, the influence of working pressure on the morphology and alignment of PCL fibers can be deduced. The alignment and uniformity of PCL fibers decreased with the increase of working pressure. Meanwhile, the

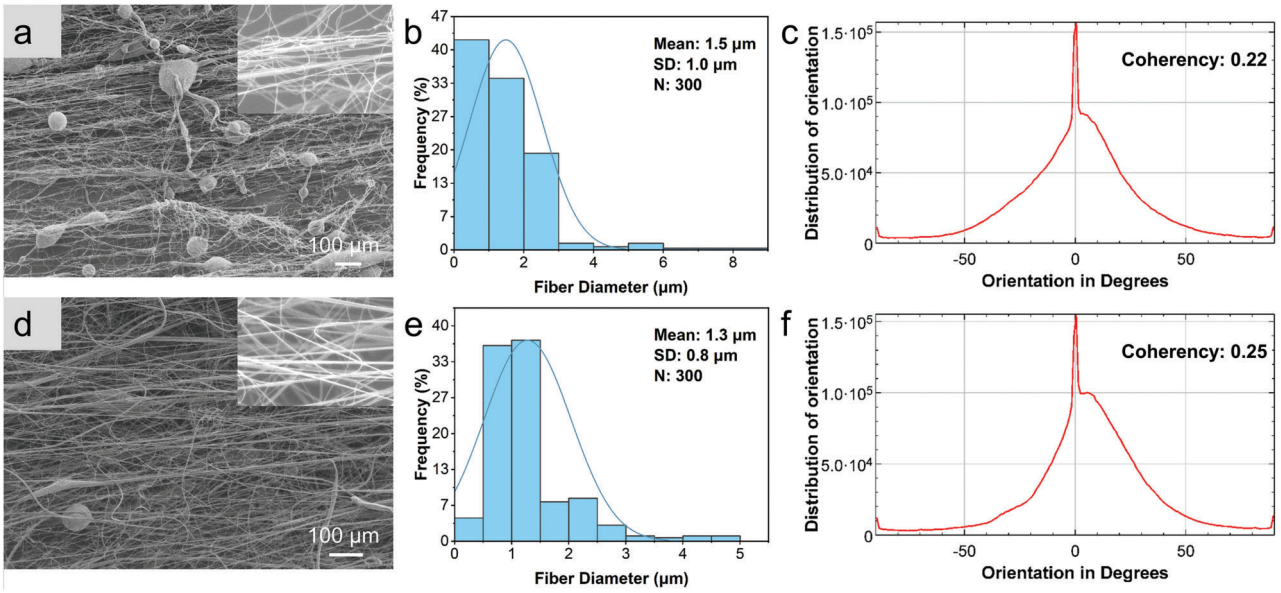

Figure 4. SEM images, fiber diameter distribution graphs, and orientation distribution graphs of PCL fibers produced by a–c) PG and d–f) nozzle-PG under 0.3 MPa working pressure. The insets show the high-magnification (×1000) SEM images of fibers.

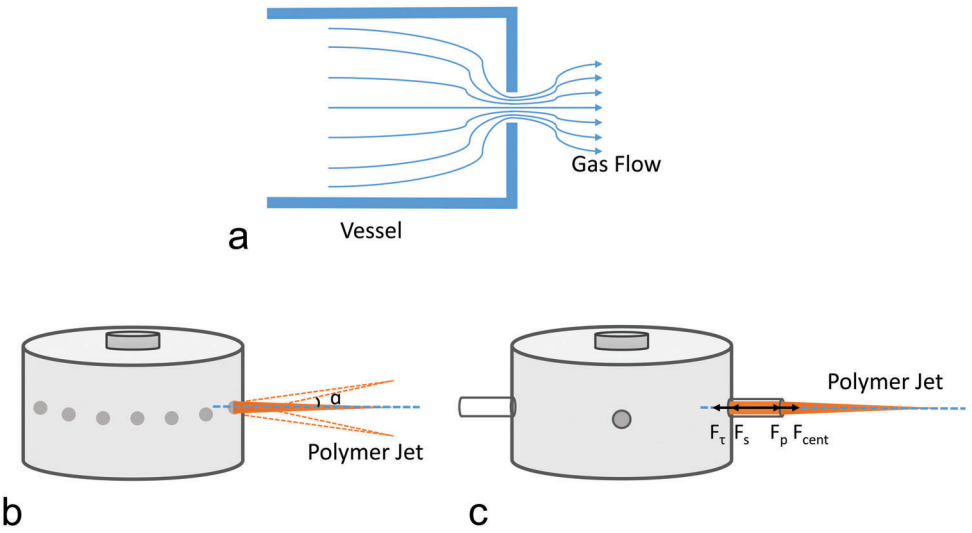

Figure 5. Diagrammatic representation of a) the gas flows through the orifice; b) the liquid flow ejected from orifices in PG; c) the liquid flow ejected from nozzles in nozzle-PG.

fiber diameter decreased accordingly from 3.9 to 1.5 µm in PG, from 2.4 to 1.3 µm in nozzle-PG. A higher working pressure is generally preferred in PG to produce finer fibers, while it significantly affects the fiber alignment and the presence of beads. This is due to the high pressure which helps to overcome the surface tension of the polymer solution loaded in the chamber to form a spinning jet with a smaller diameter, thereby generating finer fibers.[61] However, the gas flow enhances the instability of the spinning jets, resulting in the formation of beads and the low alignment of fibers.

The same experiment was carried out at 15% (w/v) PVP/ethanol. The results are shown in Figures S1–S3 (Supporting Information). Figure S1a,d shows the SEM images of PVP fibers processed by PG and nozzle-PG at 0.1 MPa working pressure, respectively. PG produced a PVP fiber mat contained large beads. In contrast, the PVP fiber mat synthesized by nozzle-PG only had some small beads. The effects of vessel geometry played a key role in the fiber diameter value. PVP fibers with the diameter of 2.9 ± 1.2 µm were manufactured at 0.1 MPa with PG, while nozzle-PG under the same working pressure generated finer and more uniform fibers with a diameter of 1.8 ± 0.7 µm. In addition, PVP fibers processed by nozzle-PG also showed better fiber alignment with a larger orientation coherency coefficient (0.36) than that of PG (0.29) at the same pressure.

These encouraging results are also replicated in the 0.2 MPa 0.3 MPa spinning of the PVP/ethanol solution (Figures S2 and

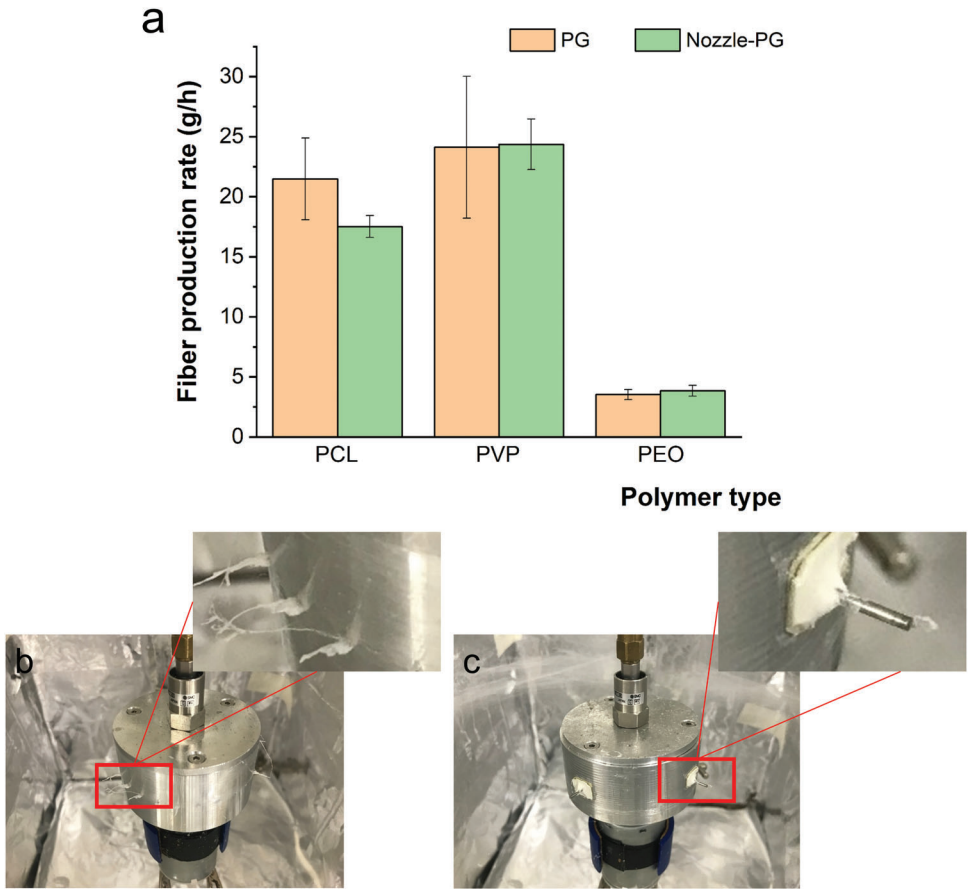

Figure 6. a) Production rate of PCL, PVP, and PEO fibers manufactured by PG and nozzle-PG under 0.1 MPa pressure. The deposition of solidified polymers in b) PG and c) nozzle-PG setup.

S3, Supporting Information). Nozzle-PG always produced finer and more aligned PVP fibers with less and smaller beads, even if working pressure changed. Although the higher pressure led to finer PVP fibers, it generated fiber mats with larger beads in nozzle-PG. The PVP fibers produced by PG and nozzle-PG under 0.3 MPa had an orientation coherency coefficient of only 0.16 and 0.19, respectively, which are $\ll 1$ (perfectly correlated). Thus, increasing working pressure can be counterproductive in the production of unidirectional fibers.

In addition to the polymers dissolved in organic solvents, the effect of vessel geometry on the spinning of water-soluble polymer PEO was also studied (Figures S4–S6, Supporting Information). Using nozzle-PG, we produced PEO nanofibers (172 ± 67 nm) with "ideal" morphology—smooth, uniform, and of better alignment than the PEO nanofibers obtained by PG (198 ± 102 nm) under 0.3 MPa working pressuring, as shown in Figure S6 (Supporting Information). In addition, no beads were observed in PEO nanofibers fabricated by nozzle-PG. The nozzle-PG processed PEO nanofibers also had the narrower distributions of fiber orientation (Figures S4f, S5f, and S6f, Supporting Information) than those of PEO nanofibers produced by PG (Figures S4c, S5c, and S6c, Supporting Information), indicating their higher fiber alignment. PG processes work better with water-based solvent polymer systems. This is because the application of pressure does not accelerate evaporation of solvent as much, if a more volatile solvent was used. Evaporation can affect fiber diameter distribution.

3.2. Fiber Production Rate

The spinning efficiency of the two gyration techniques was compared and shown in **Figure 6**. The original nozzle-free PG has a similar fiber productivity to nozzle-PG. Under the same processing parameters, PG produced 21.5 g of PCL fibers per hour. The output of nozzle-PG was 17.5 g h^{-1}. In addition, nozzle-PG reached almost the same production rate of PVP fibers as PG (≈24 g h^{-1}). PG and nozzle-PG produced PEO nanofibers with similar yield but lower efficiency, 3.5 and 3.8 g h^{-1}, respectively. Although the production rate of PEO nanofibers is lower than that of PCL and PVP in PG and nozzle-PG, it is still at least an order of magnitude higher than that of nanofibers obtained by electrospinning, which was only 0.01–0.1 g h^{-1} in single-needle electrospinning.[62] The lower yield in water soluble polymer PEO may be an artifact of its fine diameter (˂500 nm) (Figures S4–S6, Supporting Information). Thus, the collection of fibers generated was much more difficult and is envisage overcoming this problem in future work. From the error bars in Figure 6a, we can also see that nozzle-PG had a more stable fiber production rate, while the production rate of PG varied in each separate spinning. While

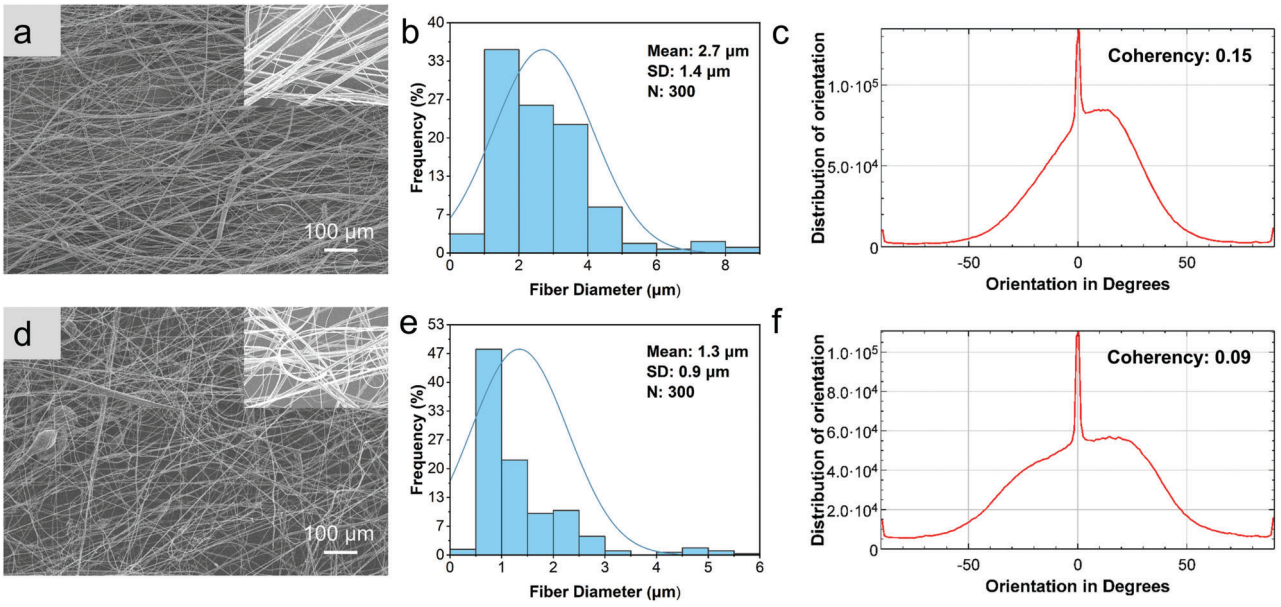

Figure 7. SEM images, fiber diameter distribution graphs, and orientation distribution graphs of PCL fibers collected at a–c) 70 mm and d–f) 130 mm in 0.1 MPa nozzle-PG. The insets show the high-magnification (×1000) SEM images of fibers. The results of PCL fibers collected at 100 mm distance are shown in Figure 2d–f.

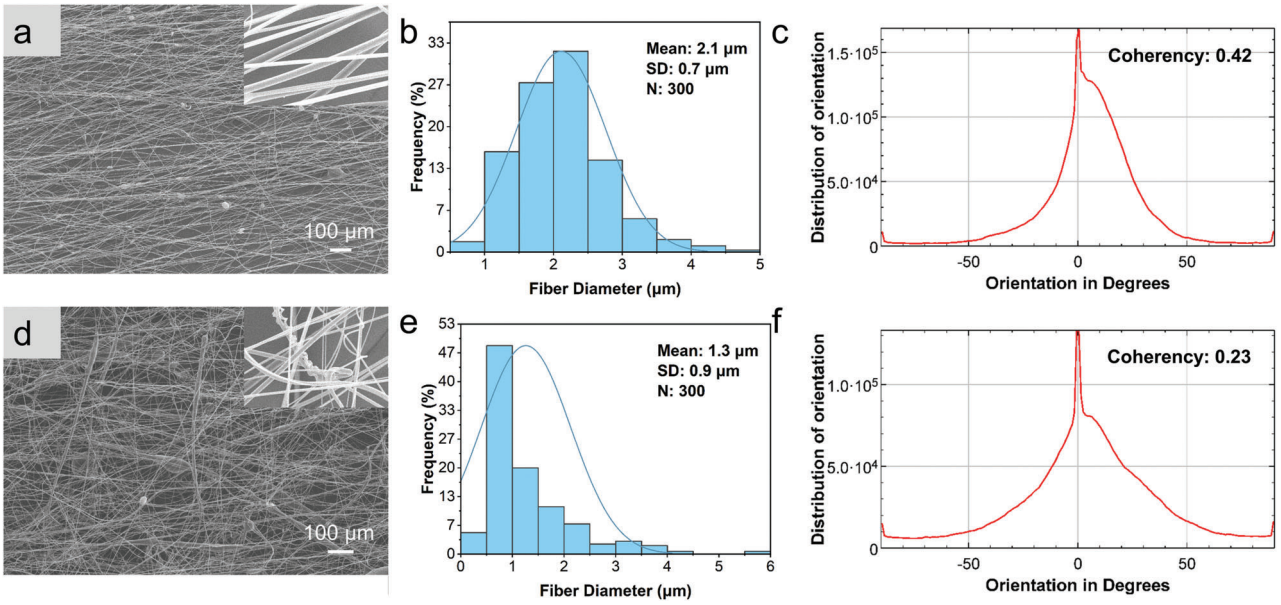

Figure 8. SEM images, fiber diameter distribution graphs, and orientation distribution graphs of PVP fibers collected at a–c) 70 mm and d–f) 130 mm in 0.1 MPa nozzle-PG. The insets show the high-magnification (×2000) SEM images of fibers. The results of PVP fibers collected at 100 mm distance are shown in Figure S1d–f (Supporting Information).

PG has more liquid channels (24 orifices) than nozzle-PG (4 nozzles), enabling the formation of more spinning jets at the same time, PG did not provide higher fiber productivity. This is due to the solution loss in PG. As the instability of solution flow occurs in PG, polymer solution is likely to aggregate and deposit at orifices instead of forming fibers (Figure 6b), which significantly reduced the quantity of fiber products. This problem can be overcome in nozzle-PG with the stable spinning jets directed by the nozzles.

3.3. Effects of Collection Distance on Fiber Morphology

The significant effects of collection distance on fiber morphology are presented in the SEM images of **Figures 7–9**. When the collection distance was 130 mm, randomly oriented PCL fibers with large beads and small diameter (1.3 ± 0.9 μm) were collected. Thicker PCL fibers were collected at 70 mm distance (2.7 ± 1.4 μm). The collection distance of 100 mm led to the best PCL fibers with pronounced fiber morphology and alignment (2.4 ±

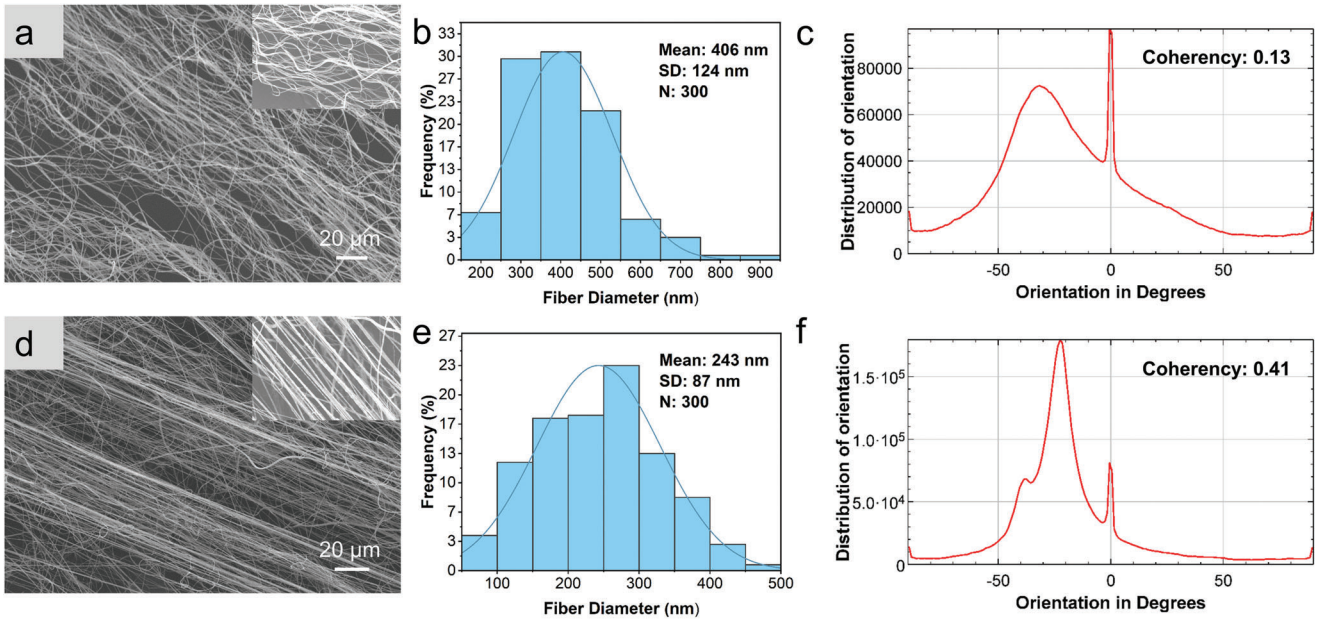

Figure 9. SEM images, fiber diameter distribution graphs, and orientation distribution graphs of PEO fibers collected at a–c) 70 mm and d–f) 130 mm in 0.1 MPa nozzle-PG. The insets show the high-magnification (×2500) SEM images of fibers. The results of PEO fibers collected at 100 mm distance are shown in Figure S4d–f (Supporting Information).

1.2 μm) (Figure 2d–f). It has been known that the spinning jet in gyrospinning undergoes stretching before reaching the collector, during which the diameter of jet decreases monotonously with the increase of movement distance.[55] Thus, it can be expected that collection distance has significant effects on fiber diameter. The polymer jet cannot be stretched sufficiently at smaller collection distances, forming short and thicker fibers. Conversely, when the collection distance is too long, it will cause jet rupture and fibers fail to deposit on the collector.[63,64] In addition, collection distance determines solvent evaporation, thus affecting the morphology of fibers. This effect may lead to different results for different polymer solution systems with different solution characteristics.

Similar results were obtained from the 0.1 MPa nozzle-PG of PVP at different collection distances. PVP fibers with different orientation were collected at 70, 100, and 130 mm collection distances, with the diameters of 2.1 ± 0.7, 1.8 ± 0.7, and 1.3 ± 0.9 μm. With the increase of collection distance, the standard deviation of fiber diameter had a slight increase, suggesting that the PVP fibers became less uniform at a longer collection distance. The result also shows that a longer collection distance is likely to produce finer PVP fibers with lower alignment. The 130 mm collection distance generated randomly arranged PVP fibers (Figure 8d), with an orientation coherency coefficient of 0.23. While the PVP fibers collected at 70 and 100 mm distance showed anisotropy with narrower orientation distributions (Figure 8c and Figure S1f, Supporting Information) and higher orientation coherency coefficients (0.42 and 0.36, respectively).

From Figures 7 and 8, it can be seen that some small beads presented as a by-product of the spinning process. The formation of beads can be the result of multiple factors, among which polymer molecular weight and polymer chain entanglement are the important ones.[10,41,65] Molecular weight that does not provide sufficient chain entanglement results in the formation of beads. For a given molecular weight, the degree of chain entanglement increases with the increase of polymer concentration.[48] Thus, a high polymer concentration helps the production of smooth and uniform fibers, while a low concentration generally promotes bead formation.[41] The bead formation is also related to centrifugal force. Beads are produced when centrifugal force is insufficient to overcome surface tension and elongate the jet before it reaches the collector.[66] This is the main reason for the beaded structure in fibers generated at a low rotational speed. In PG and nozzle-PG, the applying of high-pressure gas flow can enhance the instability of the flow state of the polymer jet, promoting the formation of beads.[10,55] The collection distance also affects bead formation. At a short collection distance, the solvent is not able to evaporate fully and solvent droplets remain on the fiber chains. These solvent droplets can prevent proper mixing of the polymer within the drying jet, resulting in the formation of beads.[45] When the collection distance is too high, excessive stretching causes jet rupture.[67] Thus, the polymer jets break up into small droplets. These droplets eventually deposit on the collector, creating polymer beads on fibers.

However, the results show some differences for water-soluble polymer PEO. As shown in Figure 9d, the PEO nanofibers collected at 130 mm distance not only showed the smallest diameter and greatest uniformity (243 ± 87 nm) than PEO nanofibers collected at 70 mm distance (406 ± 124 nm) and 100 mm distance (273 ± 72 nm), but also had aligned arrangement. Different from PCL and PVP fibers, increasing collection distance produced better PEO nanofibers with unidirectional arrangement in nozzle-PG, since it is more difficult for pure water to fully evaporate compared with organic solvents.[68] The spinning jets experience air resistance when travelling in air, during which the solvent undergoes forced convective mass transfer

on the jet surface.[69] Subsequently, the solvent evaporates to form dry fibers. The time required for this process increases as solvent volatility decreases. Thus, for aqueous solvents with lower volatility, a longer collection distance is desired to ensure the complete drying of fibers. In addition, it will extend the jet elongation to significantly reduce the fiber diameter, especially for polymers with high flexibility and high ductility such as PEO.

4. Conclusions

This work demonstrated that nozzle-PG has great potential to produce uniform fibers with smaller diameter and better alignment than original nozzle-free PG, without decreasing the fiber production rate. This very significant result held for different polymer solution systems (15% PCL/chloroform, 15% PVP/ethanol and 15% PEO/water), as well as different working pressures (0.1, 0.2, and 0.3 MPa).

In addition, this work revealed the effects of collection distance on the fiber morphology in nozzle-PG. For PCL and PVP dissolved in organic solvents, uniform fibers with small diameter and aligned arrangement were obtained at the 100 mm collection distance. For water soluble polymer, the 130 mm collection distance gave the best PEO nanofiber morphology and alignment, compared to the collection distances of 70 and 100 mm.

Overall, this study showed the tremendous prospects of nozzle-PG in mass production of fibers. Nozzle-PG achieves the efficient formation of uniform fibers with excellent alignment via a simple one-step method. These fibers have great prospects in multiple fields. It is well known that the presence of beads is a main reason of poor mechanical behavior of fibers. Uniform fibers can be used in high-efficiency filtration membranes, face masks and protective clothing due to their large specific surface area, narrow pore size and excellent mechanical properties. Aligned fibers produced by nozzle-PG have superior potential as scaffolds for tissue engineering. The parallel orientation in aligned fibers is similar to that of natural tissues (cornea, heart, nerve, skeletal muscle, etc.), which facilitates cell adhesion, migration, and proliferation. Aligned fibers that have large tensile modulus and high breaking strength are desirable for tissue engineering scaffolds. Furthermore, highly uniaxially oriented fibers can control electrodiffusion, which are promising candidates for the production of more precise biosensors. This technology can achieve the controllability of fiber morphology and orientation by changing spinning parameters. We hope to expand the scope and variety of gyrospinning vessels and to increase the number of nozzles for nozzle-PG in future research. The key aim is to achieve even higher fiber productivity. Together with original nozzle-free PG and its sister technologies, nozzle-PG adds value to polymeric fiber mass production strategies, with the potential of fiber customization for specific applications.

Supporting Information

Supporting Information is available from the Wiley Online Library or from the author.

Acknowledgements

The authors thank the UCL Mechanical Engineering workshop led by Peter Kelly for the significant contributions to the construction of the spinning vessels. Y.D. thanks the China Scholarship Council (CSC) for supporting her Ph.D. studies at University College London.

Conflict of Interest

The authors declare no conflict of interest.

Data Availability Statement

The data that support the findings of this study are available from the corresponding author upon reasonable request.

Keywords

alignment, fiber productivity, nozzles, polymers, pressurized gyration, uniformity

Received: April 18, 2022
Revised: May 13, 2022
Published online:

[1] F. Brako, B. T. Raimi-Abraham, S. Mahalingam, D. Q. M. Craig, M. Edirisinghe, *Int. J. Pharm.* **2018**, *540*, 31.
[2] K. Dziemidowicz, Q. Sang, J. Wu, Z. Zhang, F. Zhou, J. M. Lagaron, X. Mo, G. J. M. Parker, D.-G. Yu, L.-M. Zhu, G. R. Williams, *J. Mater. Chem. B* **2021**, *9*, 939.
[3] J. J. Grant, S. C. Pillai, T. S. Perova, S. Hehir, S. J. Hinder, M. Mcafee, A. Breen, *Chemosensors* **2021**, *9*, 70.
[4] J. Ahmed, M. Gultekinoglu, M. Edirisinghe, *Biotechnol. Adv.* **2020**, *41*, 107549.
[5] V. S. Naragund, P. Panda, *Emergent Mater.* **2022**, *5*, 261.
[6] C. J. Luo, S. D. Stoyanov, E. Stride, E. Pelan, M. Edirisinghe, *Chem. Soc. Rev.* **2012**, *41*, 4708.
[7] H. Ma, B. S. Hsiao, B. Chu, *ACS Macro Lett.* **2012**, *1*, 213.
[8] J. Lin, L. Xu, Y. Huang, J. Li, W. Wang, C. Feng, Z. Liu, X. Xu, J. Zou, C. Tang, *RSC Adv.* **2016**, *6*, 1253.
[9] H. Ma, C. Burger, B S. Hsiao, B. Chu, *Biomacromolecules* **2011**, *12*, 970.
[10] X. Hong, M. Edirisinghe, S. Mahalingam, *Mater. Sci. Eng., C* **2016**, *69*, 1373.
[11] R. Casasola, N. L. Thomas, A. Trybala, S. Georgiadou, *Polymer* **2014**, *55*, 4728.
[12] J. Yoon, H.-S. Yang, B.-S. Lee, W.-R. Yu, *Adv. Mater.* **2018**, *30*, 1704765.
[13] M. Pakravan, M.-C. Heuzey, A. Ajji, *Biomacromolecules* **2012**, *13*, 412.
[14] Y. Z. Zhang, Y. Feng, Z.-M. Huang, S. Ramakrishna, C. T. Lim, *Nanotechnology* **2006**, *17*, 901.
[15] K. Joy, C. W Smith, E. Hequet, S. Ed Hughs, S. Hague, *Crop Sci.* **2012**, *52*, 2089.
[16] H. Hajiali, Shahgasempour, M. R. Naimi-Jamal, H. Peirovi, *Int. J. Nanomed.* **2011**, *6*, 2133.
[17] C. J. Tan, J. J. L. Lee, B. C. Ang, A. Andriyana, G. Chagnon, M. S. Sukiman, *J. Appl. Polym. Sci.* **2019**, *136*, 47706.
[18] Z.-M. Huang, Y. Z. Zhang, S. Ramakrishna, C. T. Lim, *Polymer* **2004**, *45*, 5361.
[19] Y. Liu, Y. Ji, K. Ghosh, R. A. F. Clark, L. Huang, M. H. Rafailovich, *J. Biomed. Mater. Res., Part A* **2009**, *90A*, 1092.
[20] R. Murugan, S. Ramakrishna, *Tissue Eng.* **2007**, *13*, 1845.
[21] S. Zhong, W. E. Teo, X. Zhu, R. W. Beuerman, S. Ramakrishna, L. Y. L. Yung, *J. Biomed. Mater. Res., Part A* **2006**, *79A*, 456.

[22] M. Ottosson, A. Jakobsson, F. Johansson, *PLoS One* **2017**, *12*, e0169419.
[23] N. A. Norzain, W. C. Lin, *J. Ind. Text.* **2021**, 1528083720988127.
[24] Z. Li, S. Mei, Y. Dong, F. She, L. Kong, *Polymers* **2019**, *11*, 1550.
[25] T. Subbiah, G. S. Bhat, R. W. Tock, S. Parameswaran, S. S. Ramkumar, *J. Appl. Polym. Sci.* **2005**, *96*, 557.
[26] T. Lin, J. Fang, H. Wang, T. Cheng, X. Wang, *Nanotechnology* **2006**, *17*, 3718.
[27] A. Baji, Y.-W. Mai, S.-C. Wong, M. Abtahi, P. Chen, *Compos. Sci. Technol.* **2010**, *70*, 703.
[28] A. D. Juncos Bombin, N. J. Dunne, H. O. Mccarthy, *Mater. Sci. Eng., C* **2020**, *114*, 110994.
[29] V. Beachley, X. Wen, *Mater. Sci. Eng., C* **2009**, *29*, 663.
[30] X. Wang, X. Hu, X. Qiu, X. Huang, D. Wu, D. Sun, *Mater. Lett.* **2013**, *99*, 21.
[31] M. M. Munir, F. Iskandar, Khairurrijal, K. Okuyama, *Rev. Sci. Instrum.* **2009**, *80*, 026106.
[32] D. Li, Y. Wang, Y. Xia, *Nano Lett.* **2003**, *3*, 1167.
[33] Y. Liu, X. Zhang, Y. Xia, H. Yang, *Adv. Mater.* **2010**, *22*, 2454.
[34] P. Katta, M. Alessandro, R. D. Ramsier, G. G. Chase, *Nano Lett.* **2004**, *4*, 2215.
[35] U. Ali, H. Niu, S. Aslam, A. Jabbar, A. W. Rajput, T. Lin, *J. Mater. Sci.* **2017**, *52*, 7567.
[36] G. Chang, J. Shen, *Macromol. Mater. Eng.* **2011**, *296*, 1071.
[37] K. Sarkar, C. Gomez, S. Zambrano, M. Ramirez, E. De Hoyos, H. Vasquez, K. Lozano, *Mater. Today* **2010**, *13*, 12.
[38] Z. Mceachin, K. Lozano, *J. Appl. Polym. Sci.* **2012**, *126*, 473.
[39] B. Vazquez, H. Vasquez, K. Lozano, *Polym. Eng. Sci.* **2012**, *52*, 2260.
[40] N. Obregon, V. Agubra, M. Pokhrel, H. Campos, D. Flores, D. De La Garza, Y. Mao, J. Macossay, M. Alcoutlabi, *Fibers* **2016**, *4*, 20.
[41] S. Mahalingam, M. Edirisinghe, *Macromol. Rapid Commun.* **2013**, *34*, 1134.
[42] M. Gultekinoglu, Ş. Öztürk, B. Chen, M. Edirisinghe, K. Ulubayram, *Eur. Polym. J.* **2019**, *121*, 109297.
[43] H. Alenezi, M. E. Cam, M. Edirisinghe, *Appl. Phys. Rev.* **2019**, *6*, 041401.
[44] X. Xu, J. Luo, *Appl. Phys. Lett.* **2007**, *91*, 124102.
[45] P. L. Heseltine, J. Ahmed, M. Edirisinghe, *Macromol. Mater. Eng.* **2018**, *303*, 1800218.
[46] E. Altun, M. O. Aydogdu, F. Koc, M. Crabbe-Mann, F. Brako, R. Kaur-Matharu, G. Ozen, S. E. Kuruca, U. Edirisinghe, O. Gunduz, M. Edirisinghe, *Macromol. Mater. Eng.* **2018**, *303*, 1700607.
[47] J. Ahmed, R. K. Matharu, T. Shams, U. E. Illangakoon, M. Edirisinghe, *Macromol. Mater. Eng.* **2018**, *303*, 1700577.
[48] S. Mahalingam, S. Homer-Vanniasinkam, M. Edirisinghe, *Mater. Des.* **2019**, *178*, 107846.
[49] B. T. Raimi-Abraham, S. Mahalingam, P. J. Davies, M. Edirisinghe, D. Q. M. Craig, *Mol. Pharmaceutics* **2015**, *12*, 3851.
[50] P. L. Heseltine, J. Hosken, C. Agboh, D. Farrar, S. Homer-Vanniasinkam, M. Edirisinghe, *Macromol. Mater. Eng.* **2019**, *304*, 1800577.
[51] B. T. Raimi-Abraham, S. Mahalingam, M. Edirisinghe, D. Q. M. Craig, *Mater. Sci. Eng., C* **2014**, *39*, 168.
[52] E. Altun, M. O. Aydogdu, M. Crabbe-Mann, J. Ahmed, F. Brako, B. Karademir, B. Aksu, M. Sennaroglu, M. S. Eroglu, G. Ren, O. Gunduz, M. Edirisinghe, *Macromol. Mater. Eng.* **2019**, *304*, 1800537.
[53] E. Fonck, G. G. Feigl, J. Fasel, D. Sage, M. Unser, D. A. RüFenacht, N. Stergiopulos, *Stroke* **2009**, *40*, 2552.
[54] P. Basnett, R. K. Matharu, C. S. Taylor, U. Illangakoon, J. I. Dawson, J. M. Kanczler, M. Behbehani, E. Humphrey, Q. Majid, B. Lukasiewicz, R. Nigmatullin, P. Heseltine, R. O. C. Oreffo, J. W. Haycock, C. Terracciano, S. E. Harding, M. Edirisinghe, I. Roy, *ACS Appl. Mater. Interfaces* **2021**, *13*, 32624.
[55] H. Xu, H. Chen, X. Li, C. Liu, B. Yang, *J. Polym. Sci., Part B: Polym. Phys.* **2014**, *52*, 1547.
[56] Y. Duan, Z. Zhang, B. Lu, B. Chen, Z. Lai, *J. Eng. Fibers Fabr.* **2019**, *14*, 1558925019828207.
[57] B. L. Smith, A. Glezer, *J. Fluid Mech.* **2002**, *458*, 1.
[58] R. E. Benavides, S C. Jana, D. H. Reneker, *Macromolecules* **2013**, *46*, 6081.
[59] M. J. Divvela, An-C Ruo, Y. Zhmayev, Y. L. Joo, *J. Non-Newtonian Fluid Mech.* **2017**, *247*, 62.
[60] Z. Zhiming, C. Boya, L. Zilong, W. Jiawei, D. Yaoshuai, *Polymer* **2020**, *205*, 122794.
[61] X. Hong, S. Mahalingam, M. Edirisinghe, *Macromol. Mater. Eng.* **2017**, *302*, 1600564.
[62] N. M. Thoppey, J. R. Bochinski, L. I. Clarke, R. E. Gorga, *Nanotechnology* **2011**, *22*, 345301.
[63] X. Zhang, Y. Lu, *Polym. Rev.* **2014**, *54*, 677.
[64] S. Noroozi, W. Arne, R. G. Larson, S. M. Taghavi, *J. Fluid Mech.* **2020**, *892*, A26.
[65] R. T. Weitz, L. Harnau, S. Rauschenbach, M. Burghard, K. Kern, *Nano Lett.* **2008**, *8*, 1187.
[66] P. Mellado, H. A. Mcilwee, M. R. Badrossamay, J. A. Goss, L. Mahadevan, K. Kit Parker, *Appl. Phys. Lett.* **2011**, *99*, 203107.
[67] X. Li, Y. Lu, T. Hou, J. Zhou, A. Wang, X. Zhang, B. Yang, *J. Appl. Polym. Sci.* **2021**, *138*, 50275.
[68] J. Merchiers, C. D. V. Martínez Narváez, C. Slykas, N. K. Reddy, V. Sharma, *Macromolecules* **2021**, *54*, 11061.
[69] H. M. Golecki, H. Yuan, C. Glavin, B. Potter, M. R. Badrossamay, J. A. Goss, M. D. Phillips, K. K. Parker, *Langmuir* **2014**, *30*, 13369.

